J Biol Inorg Chem (2012) 17:951–960
DOI 10.1007/s00775-012-0911-2

ORIGINAL PAPER

Highly cytotoxic trithiophenolatodiruthenium complexes of the type $[(\eta^6\text{-}p\text{-}MeC_6H_4Pr^i)_2Ru_2(SC_6H_4\text{-}p\text{-}X)_3]^+$: synthesis, molecular structure, electrochemistry, cytotoxicity, and glutathione oxidation potential

Federico Giannini · Julien Furrer · Anne-Flore Ibao · Georg Süss-Fink · Bruno Therrien · Olivier Zava · Mathurin Baquie · Paul J. Dyson · Petr Štěpnička

Received: 20 March 2012 / Accepted: 25 May 2012 / Published online: 16 June 2012

Abstract A series of cationic dinuclear *p*-cymene ruthenium trithiophenolato complexes of the type $[(\eta^6\text{-}p\text{-}MeC_6H_4Pr^i)_2Ru_2(SC_6H_4\text{-}p\text{-}X)_3]^+$ (**1** X is H, **2** X is Me, **3** X is Ph, **4** X is Br, **5** X is OH, **6** X is NO_2, **7** X is OMe, **8** X is CF_3, **9** X is F, **10** X is Pr^i, **11** X is Bu^t) have been synthesized from the reaction of $[(\eta^6\text{-}p\text{-}MeC_6H_4Pr^i)\text{-}RuCl_2]_2$ with the corresponding thiol, isolated as the chloride salts, and further studied for their electrochemical properties, cytotoxicity towards human ovarian cancer cells, and catalytic activity for glutathione (GSH) oxidation. Complex **1** was also compared with the benzene and hexamethylbenzene analogues $[(\eta^6\text{-}C_6H_6)_2Ru_2(SC_6H_5)_3]^+$ (**12**) and $[(\eta^6\text{-}C_6Me_6)_2Ru_2(SC_6H_5)_3]^+$ (**13**). The most active compound [**11**]Cl was structurally studied by single-crystal X-ray diffraction analysis. The concentrations corresponding to 50 % inhibition of cancer cell growth (IC_{50} values) in the A2780 and A2780cisR cell lines of these complexes except for **6** were in the submicromolar range, complex **11** showing an IC_{50} value of 0.03 μM in both cell lines. The high in vitro anticancer activity of these complexes may be at least partially due to their catalytic potential for the oxidation of GSH, although there is no clear correlation between the IC_{50} values and the turnover frequencies at about 50 % conversion. However, the cytotoxicity is tentatively correlated to the physicochemical properties of the compounds determined by the electronic influence of the substituents X (Hammett constants σ_p) and the lipophilicity of the thiols $p\text{-}XC_6H_4SH$ (calculated log *P* parameters).

Keywords Ruthenium · Cancer · Cytotoxicity · Lipophilicity · Glutathione oxidation

Dedicated to Prof. Wolfgang Beck on the occasion of his 80th birthday.

Electronic supplementary material The online version of this article (doi:10.1007/s00775-012-0911-2) contains supplementary material, which is available to authorized users.

F. Giannini · J. Furrer (✉)
Department für Chemie und Biochemie, Universität Bern, 3012 Berne, Switzerland
e-mail: julien.furrer@dcb.unibe.ch

A.-F. Ibao · G. Süss-Fink (✉) · B. Therrien
Institut de Chimie, Université de Neuchâtel, 2000 Neuchâtel, Switzerland
e-mail: georg.suess-fink@unine.ch

O. Zava · M. Baquie · P. J. Dyson
Institut des Sciences et Ingénierie Chimiques, (EPFL), Ecole Polytechnique Fédérale de Lausanne, 1015 Lausanne, Switzerland

P. Štěpnička
Department of Inorganic Chemistry, Faculty of Science, Charles University in Prague, 12840 Prague 2, Czech Republic

Introduction

The field of antitumoral and antimetastatic arene ruthenium complexes was pioneered independently by Sadler [1, 2] and Dyson [3, 4], who reported the organometallic complexes $[(\eta^6\text{-}PhC_6H_5)Ru(en)Cl]^+$ (en is 1,2-diaminoethane) [5] and $[(\eta^6\text{-}p\text{-}MeC_6H_4Pr^i)Ru(P\text{-}pta)Cl_2]$ (pta is 1,3,5-triaza-7-phosphatricyclo[3.3.1.1]decane) [6] in 2001 [7]. The mode of action by which arene ruthenium complexes exert their antitumoral or antimetastatic effects is not yet fully understood. By analogy with platinum complexes, it was originally expected that DNA binding was also the main reason for the anticancer activity of these ruthenium complexes, but serum proteins have also been discussed as possible targets [8]. Although the ability of ruthenium to

bind to DNA has been demonstrated [9, 10], in particular for arene ruthenium 1,2-diaminoethane complexes [11–13], it was observed that DNA binding of ruthenium was weaker and different from that observed for platinum [14–16]. These findings suggest different modes of action depending on the type of complexes. Thus, arene ruthenium 1,3,5-triaza-7-phosphatricyclo[3.3.1.1]decane complexes have been found to inhibit thioredoxin reductase and cathepsin B [3, 4]. Indeed, bioanalytical data combined with an approximately 200 kDa crystal structure of $[(\eta^6\text{-}p\text{-}MeC_6H_4Pr^i)Ru(P\text{-}pta)Cl_2]$ binding to the nucleosome core particle show an overwhelming preference for protein binding of this compound [17]. In addition to direct DNA and protein interactions, another mode of action has been found for cytotoxic arene ruthenium iodoazopyridine complexes involving the catalytic oxidation of glutathione (GSH), which is supposed to be at the origin of their anticancer activity [18].

We recently observed that water-soluble and air-stable arene ruthenium complexes of the type $[(\eta^6\text{-arene})_2Ru_2(SR)_3]^+$ are surprisingly cytotoxic despite their inertness to ligand substitution [19], and that the most active derivative $[(\eta^6\text{-}p\text{-}MeC_6H_4Pr^i)_2Ru_2(SC_6H_4\text{-}p\text{-}Me)_3]^+$ [20] is a highly efficient catalyst for the oxidation of GSH in aqueous solution, which may explain its high cytotoxicity [21]. In this article, we report our systematic study of $[(\eta^6\text{-}p\text{-}MeC_6H_4Pr^i)_2Ru_2(SC_6H_4\text{-}p\text{-}X)_3]^+$ complexes, most of which are newly designed compounds, aiming at finding correlations between anticancer activity, catalytic GSH oxidation activity, and redox properties.

Materials and methods

Materials and analyses

The starting material $[(\eta^6\text{-}p\text{-}MeC_6H_4Pr^i)RuCl_2]_2$ [22] and the known complexes **1**–**5** (Scheme 1) [20, 23, 24] were prepared according to published methods. All other reagents were commercially available and were used without further purification. Electrospray ionization (ESI) mass spectra were obtained in positive-ion or negative-ion mode with an LCQ Finnigan mass spectrometer. Microanalyses were performed by the Mikroelementaranalytisches Laboratorium, ETH Zürich (Switzerland).

Synthesis and characterization of compounds [**6**]Cl–[**11**]Cl

The dinuclear complex $[(\eta^6\text{-}p\text{-}MeC_6H_4Pr^i)RuCl_2]_2$ (0.16 mmol, 100 mg) was heated in technical grade ethanol (50 mL). As soon as the starting material had completely dissolved, a solution of the corresponding thiophenol $p\text{-}XC_6H_4SH$ [0.98 mmol; X is NO_2 152 mg, X is OMe 120 μL, X is CF_3 129 μL, X is F 104 μL, X is $CH(CH_3)_2$ 152 μL, and X is $C(CH_3)_3$ 169 μL] in technical grade ethanol (5 mL) was added dropwise to the hot solution. The resulting mixture was refluxed for 18 h. After the mixture had cooled to 20 °C, the solvent was removed under reduced pressure. The oil obtained was purified by column chromatography on silica gel using a mixture of dichloromethane and ethanol (5:1) as the eluent. The chloride salts of cations **6**–**11** (Scheme 1) were isolated as air-stable orange to red solids and dried in vacuo.

Spectroscopic and analytical data for [**6**]Cl

Red crystalline solid, yield 75 mg (48 %) $C_{38}H_{40}N_3O_6Ru_2S_3Cl\cdot H_2O\cdot EtOH$ (1,032.61): calcd. C 46.53, H 4.69; found C 46.74, H 4.61. ESI mass spectrometry (MS) (MeOH): *m/z* 933.4 $[M]^+$. ^{1}H NMR (400 MHz, $CDCl_3$): $\delta = 8.31$ (d, $^3J = 8.0$ Hz, 6H, $SC_6H_4NO_2$), 8.20 (d, $^3J = 8.0$ Hz, 6H, $SC_6H_4NO_2$), 5.77 (d, $^3J = 6.0$ Hz, 2H, *H*–Ar), 5.63 (d, $^3J = 6.0$ Hz, 2H, *H*–Ar), 5.43 (m, 4H, *H*–Ar), 1.99 [sept, $^3J = 6.8$ Hz, 2H, $CH(CH_3)_2$], 1.68 (s, 6H, CH_3), 0.92 [d, $^3J = 6.8$ Hz, 6H, $CH(CH_3)_2$], 0.80 [d, $^3J = 6.8$ Hz, 6H, $CH(CH_3)_2$] ppm. $^{13}C\{^1H\}$ NMR (100 MHz, $CDCl_3$): $\delta = 149.1, 148.1, 135.0, 125.0, 109.7, 102.5, 86.4, 85.7, 85.5, 32.3, 25.2, 22.1, 17.9$ ppm.

Spectroscopic and analytical data for [**7**]Cl

Orange crystalline solid, yield 140 mg (93 %) $C_{41}H_{49}O_3Ru_2S_3Cl\cdot CH_2Cl_2$ (966.04): calcd. C 53.32, H 5.35; found C 53.17, H 5.96. ESI MS (MeOH): *m/z* 889.4 $[M]^+$. ^{1}H NMR (400 MHz, $CDCl_3$): $\delta = 7.79$ (d, $^3J = 8.8$ Hz, 6H, $SC_6H_4OCH_3$), 6.91 (d, $^3J = 8.8$ Hz, 6H, $SC_6H_4OCH_3$), 5.32 (d, $^3J = 6.0$ Hz, 2H, *H*–Ar), 5.19 (d, $^3J = 6.0$ Hz, 2H, *H*–Ar), 5.10 (d, $^3J = 6.0$ Hz, 2H, *H*–Ar), 5.07 (d, $^3J = 6.0$ Hz, 2H, *H*–Ar), 3.88 (s, 9H, OCH_3), 1.96 (sept, $^3J = 6.8$ Hz, 2H, $CH(CH_3)_2$), 1.62 (s, 6H, CH_3), 0.91 (d, $^3J = 6.8$ Hz, 6H, $CH(CH_3)_2$), 0.83 (d, $^3J = 6.8$ Hz, 6H, $CH(CH_3)_2$) ppm. $^{13}C\{^1H\}$ NMR (100 MHz, $CDCl_3$): $\delta = 160.1, 133.9, 128.6, 114.8, 107.3, 99.6, 85.4, 84.9, 84.7, 83.6, 55.7, 30.7, 22.7, 22.1, 17.8$ ppm.

Spectroscopic and analytical data for [**8**]Cl

Orange crystalline solid, yield 120 mg (76 %) $C_{41}H_{40}F_9Ru_2S_3Cl$ (1,037.99): calcd. C 47.46, H 3.89; found C 47.65, H 4.11. ESI MS (MeOH): *m/z* 1,002.8 $[M]^+$. ^{1}H NMR (400 MHz, $CDCl_3$): $\delta = 8.20$ (d, $^3J = 8.0$ Hz, 6H, $SC_6H_4CF_3$), 7.71 (d, $^3J = 8.0$ Hz, 6H, $SC_6H_4CF_3$), 5.77 (d, $^3J = 6.0$ Hz, 2H, *H*–Ar), 5.37 (m, 4H, *H*–Ar), 5.26 (d, $^3J = 6.0$ Hz, 2H, *H*–Ar), 1.89 [sept, $^3J = 6.8$ Hz, 2H, $CH(CH_3)_2$], 1.68 (s, 6H, CH_3), 0.89 [d, $^3J = 6.8$ Hz, 6H,

$CH(CH_3)_2$], 0.75 [d, ^3J = 6.8 Hz, 6H, $CH(CH_3)_2$] ppm. ^{19}F NMR (376 MHz, $CDCl_3$): δ = −62.5 ppm. $^{13}C\{^1H\}$ NMR (100 MHz, $CDCl_3$): δ = 142.5, 133.2, 130.5, 126.1, 125.3, 107.7, 100.3, 85.9, 85.3, 85.0, 84.1, 30.7, 22.5, 21.7, 17.8 ppm.

Spectroscopic and analytical data for [**9**]Cl

Orange crystalline solid, yield 65 mg (45 %) $C_{38}H_{40}F_3Ru_2S_3Cl{\cdot}0.25CH_2Cl_2$ (926.88): calcd. C 51.43, H 4.54; found C 51.37, H 5.04. ESI MS (MeOH): *m/z* 853.2 $[M]^+$. ^{1}H NMR (400 MHz, $CDCl_3$): δ = 7.89 (m, 6H, SC_6H_4F), 7.07 (m, 6H, SC_6H_4F), 5.49 (d, ^3J = 6.0 Hz, 2H, *H*–Ar), 5.23 (d, ^3J = 6.0 Hz, 2H, *H*–Ar), 5.16 (m, 4H, *H*–Ar), 1.89 [sept, ^3J = 6.8 Hz, 2H, $CH(CH_3)_2$], 1.58 (s, 6H, CH_3), 0.86 [d, ^3J = 6.8 Hz, 6H, $CH(CH_3)_2$], 0.75 [d, ^3J = 6.8 Hz, 6H, $CH(CH_3)_2$] ppm. ^{19}F NMR (376 MHz, $CDCl_3$): δ = −112.4 ppm. $^{13}C\{^1H\}$ NMR (100 MHz, $CDCl_3$): δ = 161.8, 134.6, 134.5, 132.9, 116.6, 116.4, 107.6, 100.1, 85.6, 85.2, 85.1, 83.9, 30.8, 22.6, 22.1, 17.9 ppm.

Spectroscopic and analytical data for [**10**]Cl

Red crystalline solid, yield 170 mg (86 %) $C_{47}H_{61}Ru_2S_3Cl{\cdot}0.5CH_2Cl_2$ (1,002.25): calcd. C 56.92, H 6.24; found C 56.96, H 6.38. ESI MS (MeOH): *m/z* 925.4 $[M]^+$. ^{1}H NMR (400 MHz, $CDCl_3$): δ = 7.79 [d, ^3J = 8.0 Hz, 6H, $SC_6H_4CH(CH_3)_2$], 7.23 [d, ^3J = 8.0 Hz, 6H, $SC_6H_4C(CH_3)_3$], 5.40 (d, ^3J = 6.0 Hz, 2H, *H*–Ar), 5.19 (d, ^3J = 6.0 Hz, 2H, *H*–Ar), 5.12 (d, ^3J = 6.0 Hz, 2H, *H*–Ar), 5.06 (d, ^3J = 6.0 Hz, 2H, *H*–Ar), 2.95 [sept, ^3J = 6.8 Hz, 3H, $SC_6H_4CH(CH_3)_2$], 1.87 [sept, ^3J = 6.8 Hz, 2H, $CH(CH_3)_2$], 1.64 (s, 6H, CH_3), 1.28 [d, ^3J = 6.8 Hz, 18H, $SC_6H_4CH(CH_3)_2$], 0.87 [d, ^3J = 6.8 Hz, 6H, $CH(CH_3)_2$], 0.72 [d, ^3J = 6.8 Hz, 6H, $CH(CH_3)_2$] ppm. $^{13}C\{^1H\}$ NMR (100 MHz, $CDCl_3$): δ = 149.6, 134.8, 132.6, 127.3, 106.7, 100.4, 85.8, 84.8, 84.3, 84.0, 33.9, 30.5, 24.0, 22.6, 22.0, 17.8 ppm.

Spectroscopic and analytical data for [**11**]Cl

Orange crystalline solid, yield 150 mg (92 %) $C_{50}H_{67}Ru_2S_3Cl{\cdot}EtOH$ (1,047.92): calcd. C 59.60, H 7.02; found C 59.46, H 7.07. ESI MS (MeOH): *m/z* 967.4 $[M]^+$. ^{1}H NMR (400 MHz, $CDCl_3$): δ = 7.78 [d, ^3J = 8.0 Hz, 6H, $SC_6H_4C(CH_3)_3$], 7.38 [d, ^3J = 8.0 Hz, 6H, $SC_6H_4C(CH_3)_3$], 5.41 (d, ^3J = 6.0 Hz, 2H, *H*–Ar), 5.20 (d, ^3J = 6.0 Hz, 2H, *H*–Ar), 5.12 (d, ^3J = 6.0 Hz, 2H, *H*–Ar), 5.06 (d, ^3J = 6.0 Hz, 2H, *H*–Ar), 1.84 [sept, ^3J = 6.8 Hz, 2H, $CH(CH_3)_2$], 1.65 (s, 6H, CH_3), 1.35 [s, 27H, $SC_6H_4C(CH_3)_3$], 0.86 [d, ^3J = 6.8 Hz, 6H, $CH(CH_3)_2$], 0.69 (d, ^3J = 6.8 Hz, 6H, $CH(CH_3)_2$) ppm. $^{13}C\{^1H\}$ NMR (100 MHz, $CDCl_3$): δ = 151.9, 134.5, 132.3, 126.2, 106.5, 100.7, 85.1, 84.6, 84.1, 84.0, 58.6, 34.9, 31.3, 30.4, 22.5, 22.0, 17.8 ppm.

X-ray crystal structure analysis of [**11**]Cl

A crystal of [**11**]Cl was mounted on a Stoe image plate diffraction system equipped with a ϕ circle goniometer, using Mo Kα graphite monochromated radiation (λ = 0.71073 Å) with ϕ range 0°–200°, an increment of 1.2°, and $D_{max}-D_{min}$ = 12.45−0.81 Å. The structure was solved by direct methods using the program SHELXS-97 [25]. The refinement and all further calculations were done using SHELXL-97 [25]. The hydrogen atoms were included in calculated positions and treated as riding atoms using the SHELXL default parameters. All nonhydrogen atoms were refined anisotropically, using weighted full-matrix least squares on F^2. Crystallographic details are summarized in Table 1. An ORTEP drawing [26] of [**11**]Cl is shown in Fig. 1.

CCDC 866470 contains the supplementary crystallographic data for this article. These data can be obtained free of charge from the Cambridge Crystallographic Data Centre via http://www.ccdc.cam.ac.uk/data_request/cif.

Table 1 Crystallographic and selected experimental data of [**11**]Cl

Chemical formula	$C_{50}H_{67}ClRu_2S_3$
Formula weight	1,001.81
Crystal system	Orthorhombic
Space group	$P2_12_12_1$
Crystal color and shape	Red block
Crystal size (mm^3)	0.21 × 0.18 × 0.17
a (Å)	11.5549 (4)
b (Å)	20.2135 (7)
c (Å)	22.2663 (8)
V ($Å^3$)	5200.6 (3)
Z	4
T (K)	293 (2)
D_c (g cm^{-3})	1.279
μ (mm^{-1})	0.782
Scan range (°)	$3.66 < 2\theta < 58.50$
Unique reflections	14,045
Reflections used [$I > 2\sigma(I)$]	11,010
R_{int}	0.0953
Flack parameter	0.02 (4)
Final *R* indices [$I > 2\sigma(I)$][a]	R_1 0.0686, wR_2 0.1079
R indices (all data)	R_1 0.0954, wR_2 0.1163
Goodness of fit	1.071
Max, min $\Delta\rho/e$ ($Å^{-3}$)	0.752, −1.014

[a] Structures were refined on F_0^2: $wR_2 = [\Sigma[w(F_0^2-F_c^2)^2]/\Sigma w(F_0^2)^2]^{1/2}$, where $w^{-1} = \Sigma F_0^2 + (aP)^2 + bP$ and $P = [\max(F_0^2,0) + 2F_c^2]/3$.

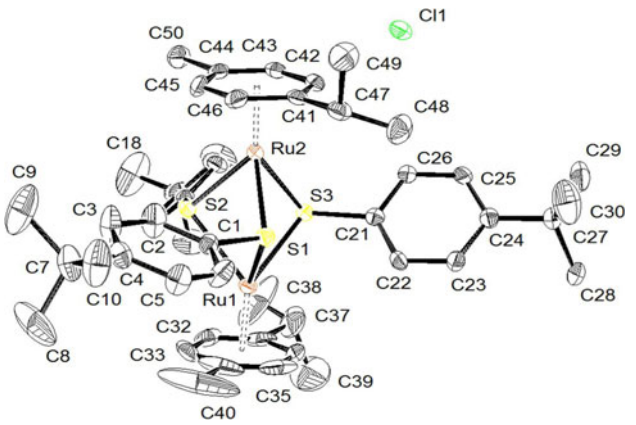

Fig. 1 ORTEP drawing of [**11**]Cl with 50 % probability level ellipsoids with hydrogen atoms omitted for clarity. Selected bond lengths (Å) and angles (°): Ru1–Ru2 3.3536(5), Ru1–S1 2.3926(15), Ru1–S2 2.4293(13), Ru1–S3 2.4015(13), Ru2–S1 2.3797(15), Ru2–S2 2.4008(12), Ru2–S3 2.4248(14); Ru1–S1–Ru2 89.29(5), Ru1–S2–Ru2 87.94(4), Ru1–S3–Ru2 88.03(5)

Table 2 Cytotoxicity of [**1**]Cl–[**13**]Cl and Cisplatin towards A2780 and A2780cisR cancer cell lines

Compound	IC_{50} for A2780 (μM)	IC_{50} for A2780cisR (μM)
[**1**]Cl	0.24 ± 0.01	0.25 ± 0.02
[**2**]Cl	0.13 ± 0.01	0.08 ± 0.03
[**3**]Cl	0.28 ± 0.03	0.10 ± 0.01
[**4**]Cl	0.25 ± 0.01	0.26 ± 0.05
[**5**]Cl	0.53 ± 0.02	1.47 ± 0.02
[**6**]Cl	26.01 ± 0.62	54.43 ± 1.38
[**7**]Cl	0.18 ± 0.03	0.15 ± 0.01
[**8**]Cl	0.17 ± 0.05	0.27 ± 0.05
[**9**]Cl	0.66 ± 0.08	1.05 ± 0.06
[**10**]Cl	0.08 ± 0.01	0.05 ± 0.01
[**11**]Cl	0.03 ± 0.01	0.03 ± 0.01
[**12**]Cl	0.37 ± 0.03	0.47 ± 0.05
[**13**]Cl	0.43 ± 0.04	1.20 ± 0.2
Cisplatin	1.35 ± 0.15	12.18 ± 0.59

IC_{50} concentration corresponding to 50 % inhibition of cancer cell growth

Electrochemistry

Electrochemical measurements were done with a μAUTOLAB III multipurpose polarograph (Eco Chemie, The Netherlands) at room temperature using a Metrohm three-electrode cell equipped with a platinum disc working electrode (2-mm diameter), a platinum sheet auxiliary electrode, and a double-junction Ag/AgCl (3 M KCl) reference electrode. The compounds were dissolved in a dry solvent (all from Sigma-Aldrich) to give a solution containing approximately 0.5 mM analyte and 0.1 M Bu_4NPF_6 (Fluka, p.a. for electrochemistry). The solutions were deaerated with argon prior to the measurement and then kept under an argon blanket. Ferrocene was used as an internal reference.

Cell culture and inhibition of cell growth

Human A2780 and A2780cisR ovarian carcinoma cells were obtained from the European Collection of Cell Cultures (ECACC, Salisbury, UK) and maintained in culture as described by the provider. The cells were routinely grown in RPMI 1640 medium with GlutaMAX^{TM} containing 5 % fetal calf serum and antibiotic (penicillin and streptomycin) at 37 °C and 5 % CO_2. For the evaluation of growth inhibition tests, the cells were seeded in 96-well plates (25×10^3 cells per well) and grown for 24 h in complete medium. The compounds were dissolved in dimethyl sulfoxide (DMSO) and added at the required concentration to the cell culture for 72 h incubation. Solutions of compounds were applied by diluting a freshly prepared stock solution of the corresponding compound in aqueous RPMI medium with GlutaMAX^{TM} (20 mM). Following drug exposure, 3-(4,5-dimethylthiazol-2-yl)-2,5-diphenyltetrazolium bromide (MTT) was added to cells at a final concentration of 0.25 mg mL^{-1} and the mixture was incubated for 2 h; then the culture medium was aspirated and the violet formazan (artificial chromogenic precipitate of the reduction of tetrazolium salts by dehydrogenases and reductases) was dissolved in DMSO. The optical density of each well (96-well plates) was quantified three times in triplicate at 540 nm using a multiwell plate reader (iEMS Reader MF, Labsystems, USA), and the percentage of surviving cells was calculated from the ratio of the absorbance of treated cells to the absorbance of untreated cells. The concentrations corresponding to 50 % inhibition of cancer cell growth (IC_{50} values) were determined by fitting the plot of the logarithmic percentage of surviving cells against the logarithm of the drug concentration using a linear regression function. The median value and the median absolute deviation were obtained using Excel^{TM} (Microsoft), and the values are reported in Table 2.

NMR spectroscopy

NMR data were acquired at 37 °C using a Bruker Avance II 500-MHz NMR spectrometer equipped with an inverse dual channel (^{1}H, X) *z*-gradient probe head (broadband inverse) or using a Bruker Avance II 400-MHz NMR spectrometer equipped with an inverse dual channel (^{1}H, X) *z*-gradient probe head (broadband inverse). One-dimensional ^{1}H NMR data were acquired with 16–64 transients as 32,768 data points over a width of 12 ppm using a classical presaturation to eliminate the water resonance. A relaxation delay of 6 s was applied between the transients. All NMR data were processed using Topspin

(version 2.1 or 3.0, Bruker, Switzerland). The ^{1}H δ scale was referenced to the residual water signal at 4.637 ppm (37 °C); the ^{13}C and ^{19}F δ scales were referenced to external tetramethylsilane and $CFCl_3$, respectively.

To evaluate the catalytic performance of the complexes for the oxidation of the reduced form of GSH to the disulfide form (GSSG) under physiological conditions, the complexes (approximately 0.2 μM) were dissolved in 0.6 mL of D_2O, and 100 equiv of GSH was added to the solution.

The samples were subsequently analyzed by ^{1}H NMR spectroscopy. For all complexes, the ^{1}H NMR spectra were recorded immediately after sample preparation, and then every 30 min until complete oxidation was evidenced by the complete disappearance of the original resonances of cysteine. To study a potential effect of the presence of chloride ions, the experiments were conducted in 4 and 50 mM D_2O solutions of NaCl.

Results and discussion

The *p*-cymene ruthenium dichloride dimer reacts in refluxing ethanol with various thiophenols to give the cationic trithiophenolato complexes $[(\eta^6\text{-}p\text{-}MeC_6H_4Pr^i)_2Ru_2(SC_6H_4\text{-}p\text{-}X)_3]^+$ (**1** X is H, **2** X is Me, **3** X is Ph, **4** X is Br, **5** X is OH, **6** X is NO_2, **7** X is OMe, **8** X is CF_3, **9** X is F, **10** X is Pr^i, **11** X is Bu^t), which can be isolated in high yields by column chromatography as air-stable chloride salts (Scheme 1). Compounds [**1**]Cl–[**5**]Cl have been reported previously [19–21, 23]. The newly prepared derivatives [**6**]Cl–[**11**]Cl were fully characterized by elemental analysis and spectroscopic methods.

The known benzene and hexamethylbenzene analogues of complex **1**, $[(\eta^6\text{-}C_6H_6)_2Ru_2(SC_6H_5)_3]^+$ (**12**) and $[(\eta^6\text{-}C_6Me_6)_2Ru_2(SC_6H_5)_3]^+$ (**13**), which were included in this study for comparison, were synthesized in the same way according to the published method [12].

Suitable crystals for X-ray analysis were obtained for the *tert*-butyl derivative [**11**]Cl by recrystallization from a chloroform/diethyl ether mixture. The molecular structure, shown in Fig. 1, contains a trigonal bipyramidal Ru_2S_3 framework, in which each ruthenium atom adopts a pseudo-octahedral geometry owing to the presence of three sulfur atoms and the *p*-cymene ligands that each formally occupies three coordination sites. Selected bond lengths and angles are listed in Fig. 1, and crystallographic details are summarized in Table 1.

The Ru–S bond distances in cation **11** range from 2.3797(15) to 2.4293(15) Å and the Ru–S–Ru angles range from 87.91(4) to 89.29(5)°, similar to those found in the known *p*-cymene derivatives $[(\eta^6\text{-}p\text{-}MeC_6H_4Pr^i)_2Ru_2(SC_6H_5)_3]^+$ [23] and $[(\eta^6\text{-}p\text{-}MeC_6H_4Pr^i)_2Ru_2(SC_6H_4\text{-}p\text{-}Br)_3]^+$ [23]. In accordance with the electron count, the Ru–Ru distance of 3.3536(5) Å is clearly outside the range for a metal–metal single bond (2.28–2.95 Å) [23].

The redox behavior of complex **2** as a representative was studied first by cyclic voltammetry in the anodic region at a platinum disc electrode using approximately 0.5 mM solutions in various dry solvents containing 0.1 M Bu_4NPF_6 as the supporting electrolyte (see the electronic supplementary material). In acetonitrile, the compound showed an irreversible anodic wave, which was followed by several relatively weaker irreversible peaks (Fig. S1). The redox response changed upon changing the solvent for the less polar, noncoordinating 1,2-dichloroethane (Fig. S2). The voltammograms recorded in this solvent were complicated owing to extensive adsorption, particularly in the case of **12** (Fig. S3), which has no substituents at the arene ring and is thus probably more prone to interactions with the electrode surface via its arene ligands.

Finally, the cyclic voltammograms of all compounds were recorded in the highly polar and donating DMSO, which is chemically more relevant to the conditions of biological testing[1]. The compounds typically displayed only one[2] single irreversible, diffusion-controlled[3] oxidation at approximately 0.66–0.78 V versus ferrocene/ferrocenium (Fig. 2). However, even these waves were probably associated with some chemical complications (e.g., adsorption phenomena) and typically shifted upon repeated scanning, which precluded any exact determination of the redox potentials. Indeed, the roughly estimated anodic peak potentials increased with the electron-withdrawing character of the substituent at position 4 of the thiophenolato ligand. However, because of uncertainty of the redox potential determination, no reliable correlation could be drawn between the redox potentials and the Hammett constants (σ_p) [27].

The antiproliferative activity of complexes **1–11** was evaluated towards the human ovarian A2780 cancer cell line and its cisplatin-resistant derivative A2780cisR using the MTT assay, which measures mitochondrial dehydrogenase activity as an indication of cell viability. The IC_{50} values of the complexes are reported in Table 2 together with those of **12**, **13**, and cisplatin, which are included for comparison.

All complexes **1–11** with exception of the nitro derivative **6** are highly cytotoxic towards human ovarian cancer cells, the IC_{50} values for the cell lines A2780 and A2780cisR being in the nanomolar range. The most active

[1] Addition of water (1 % v/v) to DMSO did not change the redox response.

[2] Some compounds (e.g., [**5**]Cl) showed complicated convoluted waves.

[3] Anodic peak currents i_{pa} increased linearly with the square root of the scan rate.

Scheme 1 Synthesis of compounds [(η^6-*p*-$MeC_6H_4Pr^i$)$_2$Ru$_2$(SC_6H_4-*p*-X)$_3$]Cl (**1** X is H, **2** X is Me, **3** X is Ph, **4** X is Br, **5** X is OH, **6** X is NO_2, **7** X is OMe, **8** X is CF_3, **9** X is F, **10** X is Pr^i, **11** X is Bu^t)

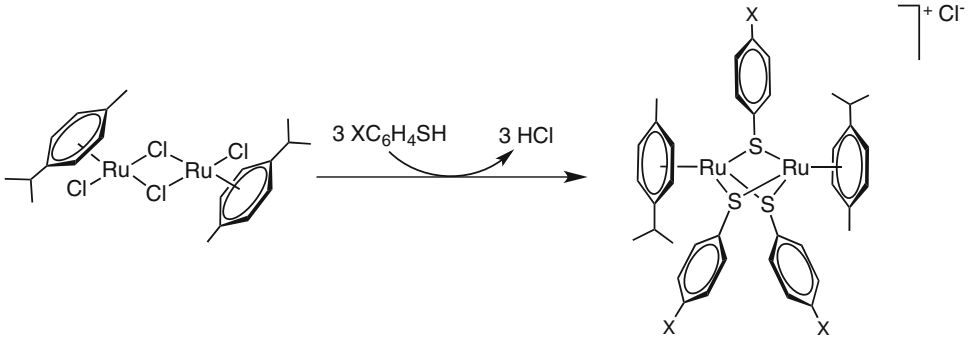

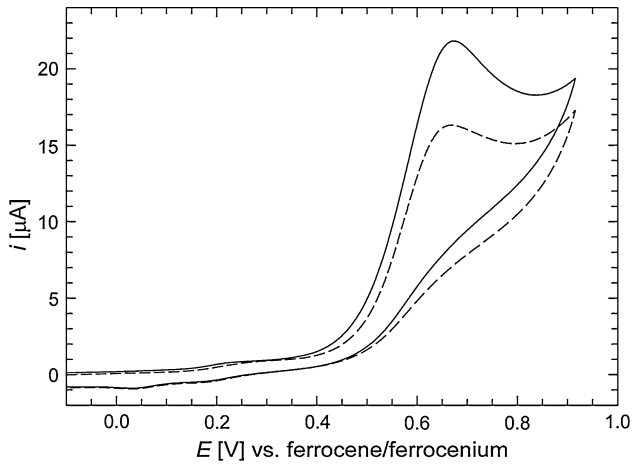

Fig. 2 Cyclic voltammograms of [**2**]Cl recorded in dimethyl sulfoxide (scan rate 0.2 V s^{-1}). *Full line* first scan, *dashed line* second scan

complex, **11**, has an IC_{50} value of 0.03 μM for both cell lines, which means that for cell line A2780 it is more than 100 times more cytotoxic than cisplatin. For the cisplatin-resistant cell line A2780cisR, complex **11** is more than 500 times more cytotoxic than cisplatin. To the best of our knowledge, these complexes are the most cytotoxic ruthenium compounds reported so far [28–31]. Such strong activity may appear surprising at first glance, since the compounds are apparently chemically inert. However, a recent study by Meier et al. [32] suggests an inverse correlation between metallodrug–protein interaction and cytotoxicity towards tumor cells. Indeed, despite their inertness towards biomolecules such as amino acids and nucleotides, complexes **1**–**11** have been found to be active catalysts for the oxidation of GSH and potentially other peptides/proteins, which could explain at least partially their biological activity.

The tripeptide GSH (Scheme 2) is the major endogenous antioxidant produced by cells (up to 5 mM in living cells). It participates directly in the neutralization of free radicals and reactive oxygen compounds, and maintains the levels of exogenous antioxidants such as vitamin C. In healthy cells, more than 90 % of the total GSH pool is present in the reduced form (GSH) and less than 10 % exists in the oxidized disulfide form (GSSG) [33, 34].

We therefore studied the possible interaction of GSH with complex **2** and found it catalyzes the oxidation of cysteine to cystine and also that of GSH to GSSG in water [21]. Here we report a systematic NMR study of the catalytic oxidative behavior of all 11 compounds, following the reaction between complexes **1**–**11** with GSH in a 1:100 ratio. The ^{1}H NMR spectra, recorded in a 4 mM NaCl solution in D_2O/DMSO-d_6 (95:5) at pD 7 and 37 °C and in an aerobic atmosphere (the GSH autoxidation in the presence of O_2 being less than 5 % in 24 h), showed that the incubation of 90 mM GSH with 0.9 mM **1**–**11** leads to the complete oxidation of GSH to GSSG in 13–16 h, as evidenced by the disappearance of the β-CH_2 resonances of GSH at $\delta \sim 3$ ppm and the simultaneous appearance of two new resonances at $\delta \sim 3.1$ ppm and $\delta \sim 3.4$ ppm, corresponding to the β-CH_2 of GSSG (see the electronic supplementary material). To study a potential effect of the presence of chloride ions, experiments were also conducted in 50 mM D_2O solutions of NaCl. The results for complexes **8**–**11** show the turnover frequencies at about 50 % conversion (TOF_{50}) increase by only about 10 % upon increasing the concentration of the chloride ions from 4 to 50 mM, thus confirming our findings for complex **2** [21].

Figure 3 shows the catalytic turnover as a function of time for the most active complex, **11**. The TOF_{50} values are listed in Table 3; they were obtained from each catalytic run by fitting the turnover frequencies as a function of time with the exponential expression $y = a - bc^x$ for all complexes. The turnover frequencies were calculated according to the following equation: $\{I_{GSSG}/(I_{GSH} + I_{GSSG})\} \times \{[GSH]_0/[complex]\}$, where I_{GSSG} and I_{GSH} are the integral intensities of the signals of GSSG and GSH respectively. The turnover frequencies were obtained as a derivative of the fitting function for $x = 2$ (after 2 h incubation corresponding to 50 % conversion of GSH to GSSG). All turnover frequencies obtained are in the range from 5.5 to 8.5 h^{-1}.

Table 3 summarizes the catalytic turnover frequencies (TOF_{50}), the Hammett constants (σ_p) of the substituents R

Scheme 2 Oxidation of reduced glutathione (GSH) to give the disulfide GSSG

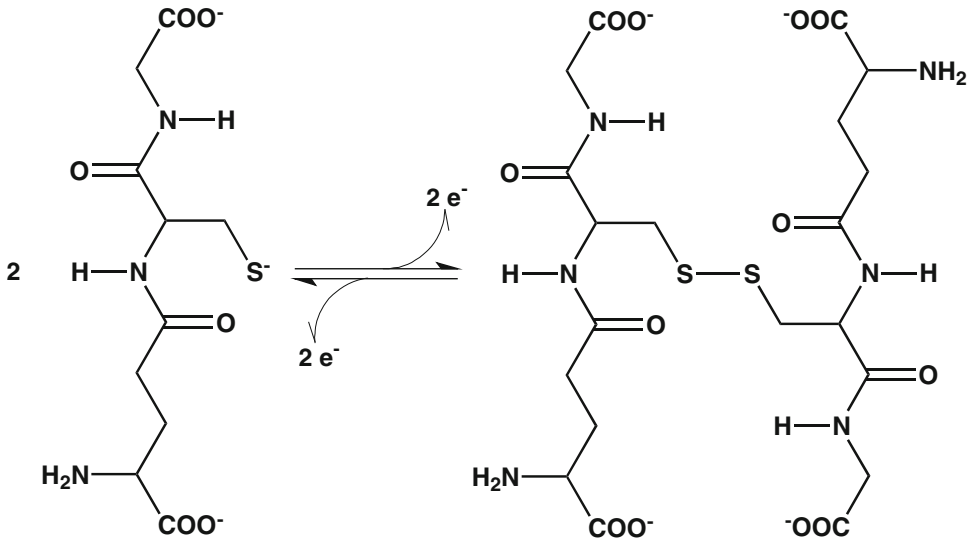

(GSH) **(GSSG)**

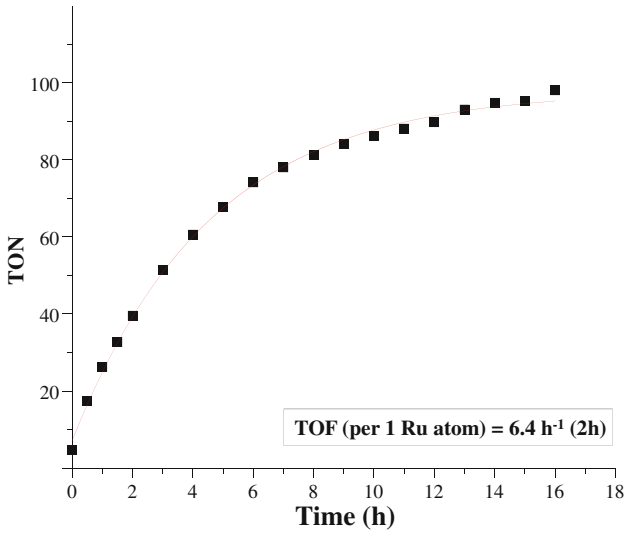

Fig. 3 Turnover frequency (TOF) of complex **11** for the catalytic oxidation of reduced glutathione

reflecting their electronic influence [27], and the calculated partition coefficients (log *P*) of the complexes reflecting their lipophilicity. The partition coefficients (log *P*) were calculated using ACD/ChemSketch [35]. As the *p*-cymene ruthenium fragments are the same in complexes **1**–**11**, the lipophilicity of these complexes should vary with the RSH log *P* parameters. Indeed, in a recent study, Achrem-Achremovicz et al. [36] showed that these calculated log *P* values match closely those obtain by experiment in the case of semisynthetic botulin derivatives, and that the values obtained can be used in correlations of biological activities of the compounds and their structures.

The data shown in Table 3 suggest there is no clear correlation between the IC_{50} values for the cytotoxicity and the TOF_{50} values for the catalytic oxidation of GSH to GSSG, presumably owing to differences in cellular uptake of the compounds, which is related to the lipophilicity (see below). For instance, the TOF_{50} value of the most cytotoxic complex of this series, complex **11** (IC_{50} = 0.03 μM towards both cell lines) drops to 6.4 h^{-1}, whereas it increases to 8.4 h^{-1} for complex **3** (IC_{50} = 0.28 μM towards A2780 cells), but goes down again to 7.5 h^{-1} for the least cytotoxic complex, **6** (IC_{50} = 26 and 54.4 μM towards A2780 and A2780cisR, respectively). This is presumably because the IC_{50} data express the anticancer activity of **1**–**11** for living cancer cells in cell culture, whereas the TOF_{50} data relate to the catalytic activity of **1**–**11** for the oxidation of GSH in an isolated system. Accordingly, there is no correlation between the TOF_{50} data and the Hammett constants (σ_p) nor with the partition coefficients (log *P*). However, such correlations can be found between the IC_{50} data and σ_p and log *P* (see below). Indeed, physicochemical properties such as electronic parameters and lipophilicity appear to have a greater influence on the activity of compounds in cells than the catalytic potential for the oxidation of GSH.

From the data in Table 3, correlations between the lipophilicity (log *P*) of the thiol ligands, the Hammett constants (σ_p) of the substituents at sulfur, and the IC_{50} values for the A2780 and A2780cisR cell lines can be extracted. In Fig. S6, the correlations between the IC_{50} values and the calculated partition coefficients (log *P*) are shown for both cell lines. It can be clearly seen that the lowest IC_{50} values are obtained for the complexes having log *P* values between 3.0 and 4.2 for the A2780 cell line,

Table 3 Comparison of cytotoxicities and catalytic activities of [**1**]Cl—[**11**]Cl with physicochemical data for the corresponding thiols (the log *P* values correspond to the values calculated for the thiol RSH groups)

Compound	IC_{50} for A2780 (μM)	IC_{50} for A2780cisR (μM)	TOF_{50} (h^{-1})[a]	σ_p (*R*)	Log*P* (RSH)
[**1**]Cl	0.24 ± 0.01	0.25 ± 0.02	7.2 ± 0.36	0.00	2.52 ± 0.28
[**2**]Cl	0.13 ± 0.01	0.08 ± 0.03	7.1 ± 0.35	−0.17	2.98 ± 0.28
[**3**]Cl	0.28 ± 0.03	0.10 ± 0.01	8.4 ± 0.42	−0.01	4.28 ± 0.33
[**4**]Cl	0.25 ± 0.01	0.26 ± 0.05	8.3 ± 0.42	0.23	3.53 ± 0.39
[**5**]Cl	0.53 ± 0.02	1.47 ± 0.02	7.3 ± 0.37	−0.37	1.68 ± 0.29
[**6**]Cl	26.01 ± 0.62	54.43 ± 1.38	7.5 ± 0.38	0.78	2.61 ± 0.30
[**7**]Cl	0.18 ± 0.03	0.15 ± 0.01	7.8 ± 0.39	−0.27	2.46 ± 0.30
[**8**]Cl	0.17 ± 0.05	0.27 ± 0.05	5.7 ± 0.29	0.54	3.49 ± 0.36
[**9**]Cl	0.66 ± 0.08	1.05 ± 0.06	7.8 ± 0.36	0.06	2.81 ± 0.39
[**10**]Cl	0.08 ± 0.01	0.05 ± 0.01	7.6 ± 0.38	−0.15	3.86 ± 0.28
[**11**]Cl	0.03 ± 0.01	0.03 ± 0.01	6.4 ± 0.32	−0.20	4.21 ± 0.29

TOF_{50} turnover frequency at about 50 % conversion

[a] It can be assumed that the main source of error for the TOF_{50} values stems from the integral extracted in the NMR spectra. This error can be rounded to 5 %, reflecting the signal-to-noise ratio of the ^{1}H NMR spectra. The χ^2 values, which represent the accuracy of the fits, are provided in the electronic supplementary material.

and between 2.8 and 4.3 for the A2780cisR cell line. A general correlation trend, indicated by the black line in Fig. S6, clearly emphasizes this correlation.

Taken together, the data shown in Figs. S6 and S7 suggest that the complexes possessing Hammett constants in the range $-0.2 < \sigma_p < 0$ and log *P* values above 3.0 have the lowest IC_{50} values, i.e., in the nanomolar region. The complexes with Hammett constants outside the optimal range ($-0.2 < \sigma_p < 0$), namely, **4**, **5**, and **8**, have significantly larger IC_{50} values than the other complexes, irrespective of their log *P* values. The fluorine-containing complex **8** (R is CF_3) is an exception, with low IC_{50} values (0.17 and 0.27 μM for A2780 and A2780cisR cells, respectively) despite having a rather high Hammett constant ($\sigma_p = 0.54$).

A three-dimensional graphical representation of the correlation between the IC_{50} values, the Hammett constants (σ_p), and the lipophilicity parameters (log *P*) for the 11 complexes is displayed in Fig. 4. Interestingly, the optimization problem admits a unique solution described by a second-order polynomial function. The regression shows a good nonlinear determination coefficient: $R^2 = 0.92$. In this representation, the optimal region encompassing the most favorable values for both the Hammett constant ($-0.2 < \sigma_p < 0$) and the log *P* values (log $P > 3.0$) leading to the lowest IC_{50} values is apparent.

Conclusions

The 11 trithiophenolatodiruthenium complexes tested are highly cytotoxic with comparable effects on both cisplatin-sensitive and cisplatin-resistant human ovarian cancer cell lines, with the exception of complex **6**. Three general trends can be extracted from the data. First, the results suggest that part of the high in vitro anticancer activity of these complexes may be due to their catalytic potential for the oxidation of GSH, as observed and proposed by Wang et al. [18]. It also appears that some other properties/mechanisms are involved since there is no correlation between the IC_{50} and TOF_{50} values. Second, the arene ruthenium complexes containing an aliphatic substituent (**1**, **2**, **10**, **11**) have higher cytotoxicities than the other complexes. Moreover, the cytotoxicity of these four complexes increases with the size of the substituent. Third, the Hammett constants and the lipophilicity parameters have a clear effect on the cytotoxicity, as shown by the correlations observed for the compounds. It is worth noting that the nanomolar IC_{50} values observed for some of these compounds place them among the most cytotoxic arene ruthenium compounds reported so far.

The lipophilicity undoubtedly plays an important role for future design of metal drugs [37, 38], and it was recently proposed that the level of activity can be correlated to some extent to physicochemical properties of the compounds, such as their $Ru^{III/II}$ redox potential and their lipophilicity [39]. It is now well accepted that most of the Ru^{III} derivatives such NAMI-A and KP-1019 are actually prodrugs that become cytotoxic only once they have been activated by reduction [40, 41]. Correlation between the Hammett constants, the lipophilicity parameters, and the cytotoxicity data for our complexes could be established but not really rationalized. As a reasonable hypothesis, one could assume that the ruthenium compounds alter in some way the behavior of certain enzymes in the cells after the formation of reactive oxygen species, with uptake by the cancer cells influenced by the lipophilicity properties. How these physicochemical properties of the ruthenium

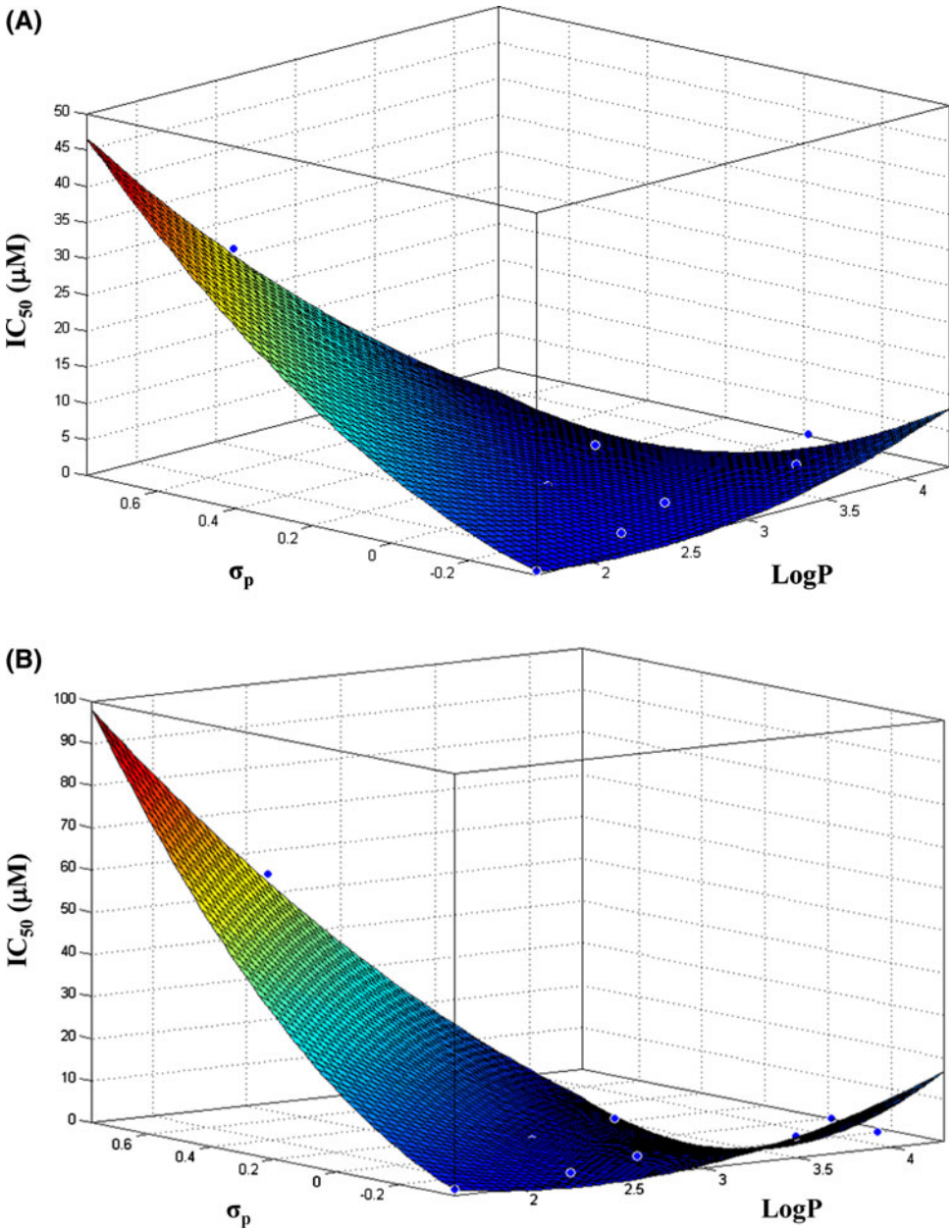

Fig. 4 Three-dimensional representation of the correlation between the concentrations corresponding to 50 % inhibition of cancer cell growth (IC_{50}), the Hammett constants (σ_p), and the lipophilicity parameters (log *P*) for the 11 ruthenium complexes. **a** A2780 cell line, **b** A2780cisR cell line. Regressions show a nonlinear determination coefficient ($R^2 = 0.92$) in both cases

compounds are responsible for the cellular oxidative power will be studied soon.

Acknowledgments This work was financially supported by the Swiss National Science Foundation (projects 200021-131867 and 200020-131844) and by the Ministry of Education, Youths and Sports of the Czech Republic (project MSM 0021620857).

References

1. Dougan SJ, Sadler PJ (2007) Chimia 61:704–715
2. Pizarro AM, Habtemariam A, Sadler PJ (2010) Top Organomet Chem 32:21–56
3. Dyson PJ (2007) Chimia 61:698–703
4. Casini A, Hartinger CG, Nazarov AA, Dyson PJ (2010) Top Organomet Chem 32:57–80
5. Morris RE, Aird RE, Murdoch PdS, Chen H, Cummings J, Hughes ND, Pearsons S, Parkin A, Boyd G, Jodrell DI, Sadler PJ (2001) J Med Chem 44:3616–3621
6. Allardyce CS, Dyson PJ, Ellis DJ, Heath SL (2001) Chem Commun 1396–1397
7. Süss-Fink G (2010) Dalton Trans 39:1673–1688
8. Melchart M, Sadler PJ (2006) In: Jaouen G (ed) Bioorganometallics, Wiley-VCH, Weinheim, pp 39–64
9. Bacac M, Hotze ACG, van der Schilden K, Haasnoot JG, Pacor S, Alessio E, Sava G, Reedijk J (2004) J Inorg Biochem 98:402–412
10. Schluga P, Hartinger CG, Egger A, Reisner E, Galanski M, Jakupec MA, Keppler BK (2006) Dalton Trans 1796–1802
11. Chen H, Parkinson JA, Morris RE, Sadler PJ (2003) J Am Chem Soc 125:173–186
12. Wang F, Chen H, Parsons S, Oswald IDH, Davidson JE, Sadler PJ (2003) Chem Eur J 9:5810–5820
13. Yan YK, Melchart M, Habtemariam A, Sadler PJ (2005) Chem Commun 4764–4776

14. Egger A, Arion VB, Reisner E, Cebrian-Losantos B, Shova S, Trettenhahn G, Keppler BK (2005) Inorg Chem 44:122–132
15. Chen H, Parkinson JA, Novakova O, Bella J, Wang F, Dawson A, Gould R, Parsons S, Brabec V, Sadler PJ (2003) Proc Natl Acad Sci USA 100:14623–14628
16. Wang F, Xu J, Habtemariam A, Bella J, Sadler PJ (2005) J Am Chem Soc 127:17734–17743
17. Wu B, Ong SM, Groessl M, Adhireksan Z, Hartinger CG, Dyson PJ, Davey CA (2011) Chem Eur J 17:3562–3566
18. Dougan SJ, Habtemariam A, McHale SE, Pearsons S, Sadler PJ (2008) Proc Natl Acad Sci USA 105:11628–11633
19. Gras M, Therrien B, Süss-Fink G, Zava O, Dyson PJ (2010) Dalton Trans 39:10305–10313
20. Chérioux F, Thomas CM, Monnier T, Süss-Fink G (2003) Polyhedron 22:543–548
21. Giannini F, Süss-Fink G, Furrer J (2011) Inorg Chem 50:10552–10554
22. Bennett MA, Huang TN, Matheson TW, Smith AK (1982) Inorg Synth 21:74–78
23. Mashima K, Mikami A, Nakamura A (1992) Chem Lett 1795–1798
24. Chérioux F, Therrien B, Süss-Fink G (2003) Eur J Inorg Chem 1043–1047
25. Sheldrick GM (2008) Acta Crystallogr A 64:112–122
26. Farrugia LJ (1997) J Appl Crystallogr 30:565
27. Hansch C, Leo A, Taft RW (1991) Chem Rev 91:165–195
28. Mendoza-Ferri MG, Hartinger CG, Eichinger RE, Stolyarova N, Severin K, Jakupec MA, Nazarov AA, Keppler BK (2008) Organometallics 27:2405–2407
29. Mendoza-Ferri MG, Hartinger CG, Nazarov AA, Kandioller W, Severin K, Keppler BK (2008) Appl Organomet Chem 22:326–332
30. Mendoza-Ferri MG, Hartinger CG, Mendoza MA, Groessl M, Egger A, Eichinger RE, Mangrum JB, Farrell NP, Maruszak M, Bednarski PJ, Klein F, Jakupec A, Nazarov AA, Severin K, Keppler BK (2009) J Med Chem 52:916–925
31. Mendoza-Ferri MG, Hartinger CG, Nazarov AA, Eichinger RE, Jakupec MA, Nazarov AA, Severin K, Keppler BK (2009) Organometallics 28:6260–6265
32. Meier SM, Hanif M, Kandioller W, Keppler BK, Hartinger CG (2012) J Inorg Biochem 108:91–95
33. Satoh N (2010) Biochem Genet 48:816–821
34. Pastore A, Lo Russo A, Greco M, Rizzoni G, Federici G (2001) Clin Chem 47:1467–1469
35. Advanced Chemistry Development (2012) ACD/ChemSketch, version 12.0. Advanced Chemistry Development, Toronto
36. Achrem-Achremowicza J, Kępczyńskab E, Zylewskib M, Janeczkoc Z (2010) Biomed Chromatogr 24:261–267
37. Scolaro C, Chaplin AB, Hartinger CG, Bergamo A, Cocchietto M, Keppler BK, Sava G, Dyson PJ (2007) Dalton Trans 5065–5072
38. Renfrew AK, Juillerat-Jeanneret L, Dyson PJ (2011) J Organomet Chem 696:772–779
39. Fetzer L, Boff B, Ali M, Meng XJ, Collin JP, Sirlin C, Gaiddon C, Pfeffer M (2011) Dalton Trans 40:8869–8878
40. Gianferrara T, Brastos I, Alessio E (2009) Dalton Trans 7588–7598
41. Bergamo A, Gaiddon C, Schellen JHM, Beijnen JH, Sava G (2012) J Inorg Biochem 106:90–99